Imaging High-Energy Electrons Propagating in a Crystal

Joanne Etheridge,[1,2,*] Sorin Lazar,[3,4] Christian Dwyer,[1,2,5] and Gianluigi A. Botton[4]

[1]*Monash Centre for Electron Microscopy, Monash University, Victoria 3800, Australia*
[2]*Department of Materials Engineering, Monash University, Victoria 3800, Australia*
[3]*FEI Electron Optics, 5600 KA Eindhoven, The Netherlands*
[4]*Canadian Centre for Electron Microscopy and Department of Materials Science and Engineering, McMaster University, Hamilton, Ontario, Canada*
[5]*ARC Centre of Excellence for Design in Light Metals, Monash University, Victoria 3800, Australia*

(Received 20 December 2010; revised manuscript received 18 February 2011; published 18 April 2011)

It has recently become possible to focus a beam of high-energy electrons to a spot smaller than an atom, with vast potential for the study of condensed matter. We devise an experiment that can image, with subangstrom resolution, the distribution of such an electron beam as it scatters within an atomic lattice. Our experiments reveal the acute sensitivity of the scattered electron distribution to 0.1 Å shifts of the impact point. Scattering due to plasmon excitations is also examined. Implications for the study of the atomic and electronic structure of condensed matter are discussed.

DOI: 10.1103/PhysRevLett.106.160802 PACS numbers: 07.78.+s, 61.05.J−, 68.37.Ma, 79.20.Uv

Recent advances in electron optics have enabled high-energy electron beams to be focused to a spot smaller than an atom [1,2]. These are being used in scanning transmission electron microscopes to image the atomic structure of condensed matter with subangstrom resolution [3–8], bringing fundamental new insights into structure-property relationships across the physical sciences; see, for example, [8–16]. Here we devise experiments to image, for the first time, the distribution of a high-energy atomic-sized electron beam after scattering by atoms inside a crystal. The images resolve detail smaller than an angstrom, revealing the relationship between the incident beam position and the scattered electron distribution and identifying which atoms are ''sampled'' by the beam. We also extend this method to measure the distribution of electrons that have excited a plasmon for different positions of the incident beam within a unit cell of LaB_6. This offers a new approach for characterizing the local atomic structure of materials with the prospect of isolating information from individual atoms.

The experimental concept is illustrated in Fig. 1. A beam of high-energy electrons is focussed to a spot smaller than an atomic radius. This electron beam is positioned at selected lattice sites on or between atoms within a foil of gold, approximately 60 atoms thick. The electrons scatter strongly from the electrostatic potential of the gold, and the resulting distribution of scattered electrons is imaged in ''real'' (or ''coordinate'') space, at better than atomic resolution. The optical plane at which this image is in focus can be selected and is chosen to be the same as the focal plane of the incident electron beam.

This electron-optical configuration takes advantage of a new generation of ultrastable transmission electron microscope (TEM) fitted with an ''aberration corrector'' [1,17] on both the probe and image forming lens systems. The ''probe corrector'' enables the formation of an electron beam the order of 1 Å in diameter, while the ''image corrector'' ensures the faithful transfer of the scattered beam onto the image plane with better than 1 Å resolution (see supplementary material [18]).

Figure 2 shows an example of the experimental sequence and output using an incident electron beam with

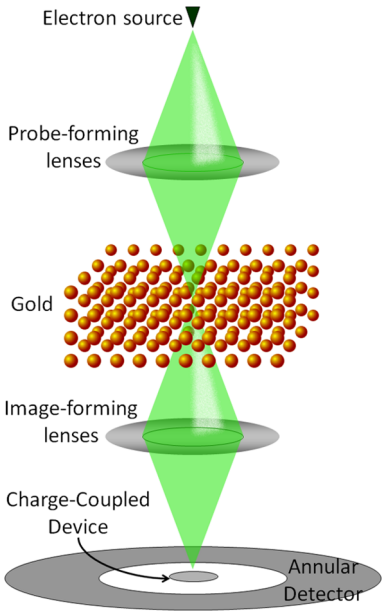

FIG. 1 (color online). Schematic of the experimental configuration. An electron beam, smaller than an atom, is focused onto or between atoms in gold. The resulting distribution of scattered electrons inside the gold crystal is imaged in the image plane revealing features at subangstrom resolution. (The image is recorded with the charge-coupled device). An annular RSTEM image can be formed by scanning this beam and recording the intensity reaching the annular detector at each scan position.

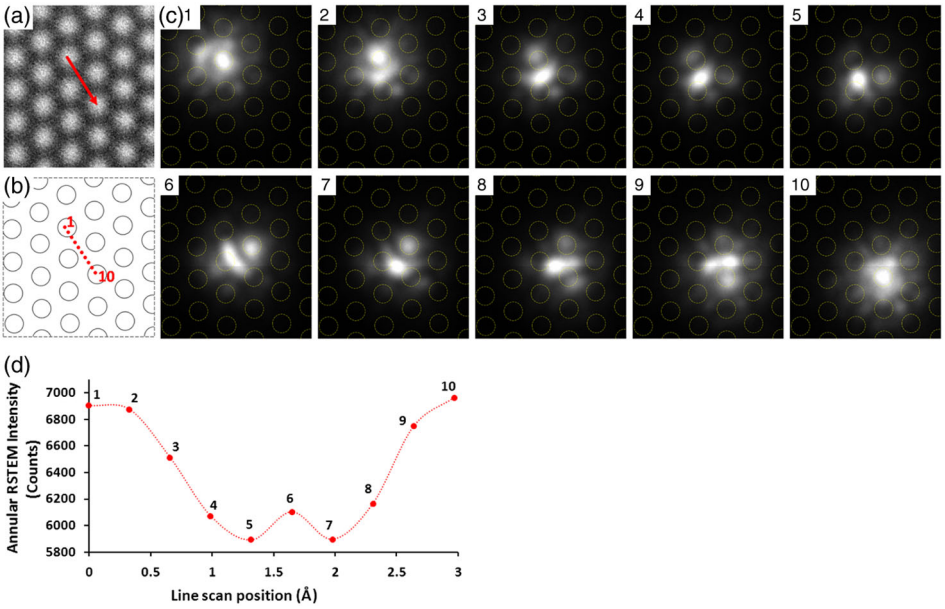

FIG. 2 (color online). Imaging the intensity distribution in real space of an electron beam after scattering from gold (140 Å thick, ⟨111⟩ orientation). [Circles mark atomic positions and correspond to 1 Å diameter. a)–(c) are scaled equivalently.] (a) Annular RSTEM image used to "map" atomic positions. Arrow marks the path along which the incident beam was scanned, as labeled in (b). (c) Intensity distribution in real space of the electron beam after scattering from gold, corresponding to the incident beam positions (1)–(10) in (b). (d) Number of electrons counted by the annular detector in real space at each incident beam position.

a 1.3 Å FWHM (see supplementary material for experimental conditions [18]). In the first part of the experiment, the position of atomic columns in the crystal with respect to the electron beam position must be established. We achieve this by using a new imaging method (see supplementary material [18] and [19]) which we have called "real space scanning transmission electron microscopy" or RSTEM. RSTEM images are created by inserting detectors centered on the optic axis in the image, or real space, optical plane and then measuring the integrated signal at each point as the electron beam is scanned across the specimen (Fig. 1). For the present task, we use a detector in the geometry of an annulus. The annular RSTEM imaging mechanism generates intensity maxima at atomic positions (see supplementary material [18]). This enables us to map the position of the atomic columns [Fig. 2(a)] and then position the electron beam with respect to these, without having to alter the precisely configured optical alignment required for the primary experiment.

Equipped with this "map" of atomic positions [Fig. 2(a)], the electron beam is scanned along a line nominally between two equivalent symmetry points within the crystal's unit cell, as specified on the annular RSTEM image [Fig. 2(a)] and labeled on the schematic [Fig. 2(b)]. The resulting scattered intensity distribution [Fig. 2(c)] of the propagated beam was recorded at approximately 0.3 Å steps during the scan using a charge-coupled device located on the optic axis (Fig. 1). At the same time, the intensity hitting the annular detector was recorded [Fig. 2(d)], in order to monitor for any deviation from the path prescribed in the original RSTEM image and unequivocally relate the position of the beam with the atomic position at each point in the line scan. The experiments were conducted in ultrastable environments [20,21] and we found that the experimental observations were reproducible over many similar scans.

Figure 2(c) shows the resulting images of the scattered electron intensity distribution versus electron beam position. These experiments enable us to "see inside" the crystal and visualize exactly how the electrostatic potential modulates the incident focused wave field. The images represent the intensity distribution at the exit face of the crystal imaged at the focal plane of the incident electron beam, given by (ignoring aberrations)

$$I(x,y) = |\Psi(x,y)|^2 = \left| \Psi_{\text{exit}}(x,y) \otimes \exp\frac{ik(x^2+y^2)}{4\pi\Delta z} \right|^2,$$

where $\Psi_{\text{exit}}(x,y)$ is the wave function in coordinate space at the exit face of the crystal and Δz is the distance from the exit face to the focal plane of the imaging system, which is coincident with the focal plane of the incident beam. In other words, the image represents the intensity distribution of the exit wave function after undergoing Fresnel diffraction back to the chosen conjugate image plane, which in this case lies within the crystal and is coincident with the focal plane of the incident beam.

The diameter of the incident electron beam used here (1.3 Å FWHM) is comparable to the atomic radius of a gold atom. It is evident that the scattered intensity

distribution is acutely sensitive to even 0.3 Å shifts in beam position, even though the beam itself is about 4 times larger in diameter. When the electron beam is positioned at a point of high crystallographic symmetry, this fact is reflected in the resultant scattered electron distribution, such as the images taken near the sixfold, threefold, and twofold sites in Fig. 2(c), image (10), images (5) and (7), and image (6), respectively.

Crucially, these images provide the first direct experimental evidence that the electron probe rapidly disperses onto and between the atomic columns adjacent to the initial probe position, as has been predicted by theory [22–26]. This understanding is vital for deriving structural and bonding information about the specimen at the highest possible spatial resolution from conventional atomic resolution STEM images and electron energy-loss (EEL) spectra. Conventional STEM images and EEL spectra provide images of the position, composition, and bonding of atomic columns projected in the electron beam direction. To extract information about the structure, composition, and bonding in the third dimension (along the beam direction) from these two-dimensional data sets, it is critical to understand from which atoms the incident electron beam has scattered. These images of the electron distribution equip us with the information necessary to derive high-resolution three-dimensional structural information from these two-dimensional data sets.

It is possible to relate the scattered intensity distribution in real space [Fig. 2(c)] with the intensity reaching the annular detector in real space from the corresponding annular RSTEM line profile [Fig. 2(d)]. For example, it is evident that the greatest intensity reaches the annular detector when the beam is located on the atom column [Fig. 2(c), images (1) and (10)], where it is expected there is the largest change in transverse momentum, and hence, position at the exit plane (due to a higher probability of phonon and Rutherford scattering—see supplementary material [18]). Similarly, the intensity is at its lowest when the beam is at the midpoint between three nearest-neighbor atoms and furthest from any atom. In addition, there is a small local maximum when the beam is located at the midpoint between two nearest-neighbor atoms, where the nearest atoms are not quite as far as in the threefold case. The corresponding image of the scattered electron distribution reveals that there is some scattering onto the atoms adjacent to the beam position, giving rise to the local maximum, even though the incident beam is positioned away from an atomic column. These experiments prove directly that the change in transverse momentum, and hence position, decreases as the beam moves away from an atom core.

To verify our interpretation of these images, the electron intensity distribution in real space was calculated using parameters consistent with the experimental conditions used in Fig. 2 (see supplementary material [18]). The

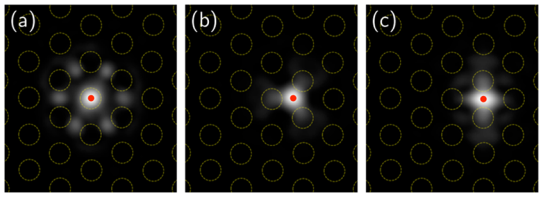

FIG. 3 (color online). Computed electron intensity distribution in real space of an electron beam after scattering from gold in the ⟨111⟩ orientation, calculated using parameters consistent with the experimental conditions in Fig. 2. Panels (a)–(c) correspond to different incident electron beam positions, as marked by the red spot, being the sixfold, threefold, and twofold symmetry sites, respectively. Circles indicate atomic positions and are 1 Å in diameter.

calculations shown in Figs. 3(a)–3(c) correspond to different incident electron beam positions, the sixfold, threefold, and twofold symmetry sites, respectively, and are consistent in form with the corresponding experimental images in Fig. 2(c) [images (10), (5) and (7), and (6), respectively].

As an extension of the experiments described above, images were obtained of the distribution in real space of high-energy electrons associated with the excitation of a plasmon in a LaB_6 specimen. These images were obtained by inserting an energy-filtering slit centered on the plasmon energy loss at 29 eV (Fig. 4). As before, the probe and imaging systems were focused on the same plane with respect to 300 keV electrons. However, in this case the final images are generated by scattered electrons with a

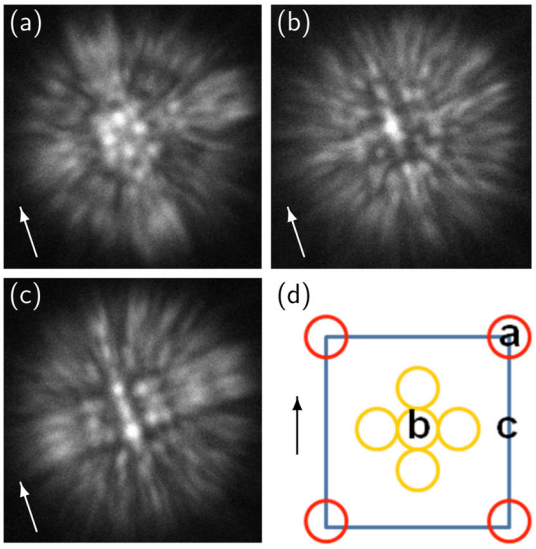

FIG. 4 (color online). Intensity distribution in real space of the electron beam after scattering from the 29 eV plasmon in ⟨100⟩ LaB_6. Panels (a)–(c) correspond to the incident beam positions indicated in the schematic (d) which shows the LaB_6 structure in the ⟨100⟩ projection. Dark gray (red) circles indicate lanthanum atoms, light gray (yellow) circles indicate boron atoms. The arrow in each figure marks the ⟨100⟩ direction.

different wavelength to the incident electron beam, so that the resulting images are defocused with respect to those presented earlier. The resultant intensity distribution reflects the symmetry of the initial-state elastically scattered wave function which created the plasmon excitation [27]. The local site symmetry of the incident probe position is clearly evident in the resultant image of the distribution of plasmon-scattered electrons. This observation is in agreement with the notion of a plasmon as a quantum excitation that is delocalized on the scale of the crystal lattice, that is, an entity without atomic-scale features. The scattering from such a delocalized excitation does not introduce significant changes in the atomic-sized electron wave field; hence, the local site symmetry of the elastically scattered wave function is preserved in the plasmon-filtered images [27].

In summary, we have imaged, for the first time and with subangstrom resolution, the distribution in real space of a high-energy electron beam that has been scattered by atoms inside a crystal. These results provide new insights into the physics of electron scattering in matter. In particular, the images reveal where the electrons are scattered within the lattice relative to their initial position, identifying exactly which atoms within the specimen they interact with. We also measured the distribution of electrons that have excited a plasmon inside a LaB_6 crystal.

Imaging the electron distribution in real space at subangstrom resolution offers an entirely different way to harness information about the specimen and introduces the possibility of identifying information from specific atoms inside a material.

These images also provide critical information for the interpretation of conventional electron microscope images and electron energy-loss spectra (EELS). While conventional atomic resolution STEM images and EELS maps are extremely powerful, providing striking two-dimensional images, the ultimate goal is to characterize individually each of the atoms within the three-dimensional atomic structure. This requires a precise understanding of how the electron beam scatters and propagates within matter so that we can correlate atomic and electronic structure images with the specific atoms that have generated the image, enabling the extraction of atomic- and electronic-structural information at the highest resolution in three dimensions. It is anticipated that this new imaging method will advance the understanding of atomic-scale structural features in condensed matter, with significant applications across the physical sciences and materials research.

Experimental work presented here was performed at the Canadian Centre for Electron Microscopy (CCEM) and at the Monash Centre for Electron Microscopy (MCEM). The CCEM is a national facility supported by the Natural Sciences and Engineering Research Council of Canada and McMaster University. Instrumentation used at MCEM was supported by the Australian Research Council infrastructure Grant No. LE0454166. G. A. B. is grateful to NSERC for a Discovery Grant for supporting this work. J. E. and G. A. B. are grateful to Ministry of Research and Innovation of Ontario for a joint ISOP grant.

*joanne.etheridge@monash.edu

[1] M. Haider *et al.*, Ultramicroscopy **75**, 53 (1998).
[2] O. L. Krivanek, N. Dellby, and A. R. Lupini, Ultramicroscopy **78**, 1 (1999).
[3] P. E. Batson, N. Dellby, and O. L. Krivanek, Nature (London) **418**, 617 (2002).
[4] P. D. Nellist *et al.*, Science **305**, 1741 (2004).
[5] H. Sawada *et al.*, Jpn. J. Appl. Phys. **46**, L568 (2007).
[6] R. Erni *et al.*, Phys. Rev. Lett. **102**, 096101 (2009).
[7] O. L. Krivanek *et al.*, Nature (London) **464**, 571 (2010).
[8] D. A. Muller, Nature Mater. **8**, 263 (2009).
[9] K. A. Mkhoyan *et al.*, Science **312**, 1354 (2006).
[10] K. Kimoto *et al.*, Nature (London) **450**, 702 (2007).
[11] N. Shibata *et al.*, Science **316**, 82 (2007).
[12] H. Ohta *et al.*, Nature Mater. **6**, 129 (2007).
[13] M. H. Gass *et al.*, Nature Nanotech. **3**, 676 (2008).
[14] J. E. Allen *et al.*, Nature Nanotech. **3**, 168 (2008).
[15] Xiulei Ji *et al.*, Nature Chem. **2**, 286 (2010).
[16] M. Heggen, L. Houben, and M. Feuerbacher, Nature Mater. **9**, 332 (2010).
[17] M. Haider *et al.*, Nature (London) **392**, 768 (1998).
[18] See supplemental material at http://link.aps.org/supplemental/10.1103/PhysRevLett.106.160802 for details of the experimental method, calculations and the RSTEM contrast mechanism.
[19] S. Lazar *et al.* (to be published).
[20] http://ccem.mcmaster.ca/about-construction.php.
[21] http://www.mcem.monash.edu.au/facilities/newbuilding.html.
[22] C. Dwyer and J. Etheridge, Inst. Phys. Conf. Ser. **168**, 127 (2001).
[23] K. Ishizuka, J. Electron Microsc. **50**, 291 (2001).
[24] C. Dwyer and J. Etheridge, Ultramicroscopy **96**, 343 (2003).
[25] C. J. Rossouw *et al.*, Ultramicroscopy **96**, 299 (2003).
[26] P. Voyles, J. L. Grazul, and D. A. Muller, Ultramicroscopy **96**, 251 (2003).
[27] P. E. Batson, Phys. Rev. Lett. **70**, 1822 (1993)